Engineering Science and Technology, an International Journal 21 (2018) 77–88

HOSTED BY

Contents lists available at ScienceDirect

Engineering Science and Technology, an International Journal

journal homepage: www.elsevier.com/locate/jestch

Full Length Article

# Numerical study on effect of boundary layer trips on aerodynamic performance of E216 airfoil

B.K. Sreejith *, A. Sathyabhama

*Department of Mechanical Engineering, National Institute of Technology Karnataka, Mangalore, Karnataka 575025, India*

ARTICLE INFO

*Article history:*
Received 8 November 2017
Revised 31 January 2018
Accepted 5 February 2018
Available online 10 February 2018

*Keywords:*
Airfoil
Boundary layer trips
Intermittency
Laminar separation bubbles
Wind tunnel

ABSTRACT

Simulation is carried out to find the performance of airfoil E216 using Transition $\gamma - Re_\theta$ model at Reynolds number of 100,000. Flow behaviour and effect of angle of attack (AOA) on laminar separation bubble (LSB) formation are examined. The results are validated with wind tunnel experimental results. LSB formation is clearly spotted in the velocity vector plot and coefficient of pressure distribution over airfoil. LSB moved upstream towards the leading edge with increase in AOA. Effect of boundary layer trip on LSB formation over the airfoil and performance of airfoil are studied. Two different trip locations, 17% of chord and 10% of chord from leading edge, and different trip heights (0.3 mm, 0.5 mm, 0.7 mm, 1 mm) are investigated in this study. Results showed that boundary layer trip could eliminate LSB partially or completely and improve aerodynamic performance of the airfoil. Maximum improvement in drag by 15.48% and lift to drag ratio by 21.62% are obtained at angle of attack of $6^0$. In all the cases, improvement in performance is observed only up to trip height of 0.5 mm.



## 1. Introduction

Renewable energy sources are becoming popular in the energy sector and wind energy is one of the fastest growing sustainable energy resources. Small scale wind turbines (SSWTs) are the systems with rotor swept area $\leqslant 200m^2$ with generated power $\leqslant 50kW$ [1]. SSWTs are preferred for low windy sites as independent or micro grid feeders [2,3] and can be installed even in remote locations where conventional power sources cannot be adopted. Poor wind velocity spectrum in the site and small rotor area of the turbine, make it to operate in-low Reynolds number (Re) ($10^4 \leqslant Re \leqslant 10^5$) [4,5]. In low Reynolds number (Re) flow, the flow is initially laminar and attached over the airfoil. Low energy in such flows creates high adverse pressure gradient (APG) making the laminar boundary layer to separate from the airfoil surface. The separated shear layer is unstable and makes transition from a laminar to turbulent shear layer. Once the turbulent shear layer has gained sufficient energy, separated flow reattaches to the airfoil surface as turbulent boundary layer, leaving a dead or re-circulating air zone between separation point and reattachment point, called laminar separation bubble (LSB) [6]. The LSB formation induces pseudo thickness to airfoil surface and increases airfoil drag which deteriorates aerodynamic performance of SSWT [7]. By mitigating LSB formation, aerodynamic performance of the SSWTs can be improved [8].

The most effective methods of LSB elimination currently in use involve, forcing premature turbulent transition of the boundary layer by means of vortex generators making it less likely to separate [9]. Many flow control methods are being developed to reduce the effects of the LSB and improve the aerodynamic performance of airfoils [10]. Passive flow control methods such as grits, wires, boundary layer trips (BLT) and dimples are the most acceptable techniques for wind turbine application due to its less complexity compared to active flow control methods. Key idea of the passive techniques is to trip the boundary layer – forcing the boundary layer from a laminar state into a turbulent state, to re-energize the flow so that the flow remains attached. BLT is a kind of obstacle in the flow which causes flow disturbance and convert laminar flow to turbulent, prior to LSB formation [11]. Many researchers studied the performance and effectiveness of different kind of BLT on various airfoils at different flow condition. Tim et al. [12] tested Clark Y12 airfoil with BLT in various chord-wise locations and at different Re between 62,000 and 209,000. They found that for higher Re any BLT applied to the airfoil caused significant increase in drag than lift and the use of BLT is restricted up to Re 135,000. Bai et al. [13] and Gopalarathnam et al. [11] also reported similar results. In a low Re study ($40,000 \leqslant Re \leqslant 1,20,000$)

* Corresponding author.
*E-mail addresses:* srijithbk@gmail.com, srijithbk.me13f08@nitk.edu.in (B.K. Sreejith).

Peer review under responsibility of Karabuk University.

https://doi.org/10.1016/j.jestch.2018.02.005
2215-0986/

*List of symbols*

| | |
|---|---|
| $c$ | Chord length,m |
| $C_p$ | Coefficient of pressure |
| $C_d$ | Drag coefficient |
| $C_l$ | Lift coefficient |
| $C_n$ | Normal force coefficient |
| $h$ | Pressure head in column of water, m |
| $k$ | Turbulent kinetic energy, $m^2/s^2$ |
| $Re$ | Reynold number based on chord length |
| $Re_\theta$ | Momentum thickness Reynolds number |
| $Re_{\theta c}$ | Critical Reynolds number |
| $Re_{\theta t}$ | Transition onset momentum thickness Reynolds number |
| $\widetilde{Re}_{\theta t}$ | Local transition onset momentum thickness Reynolds number |
| $Re_v$ | Strain rate (vorticity) Reynolds number |
| $Re_T$ | Viscosity ratio Reynolds number |
| $S$ | Strain rate |
| $x/c$ | Axial distance over airfoil along axial chord |
| $y^+$ | Non dimensional wall distance |

*Greek symbols*

| | |
|---|---|
| $\alpha$ | Angle of attack, $^0$ |
| $\gamma$ | intermittency |
| $\mu_t$ | Eddy viscosity, $m^2/s$ |
| $\mu$ | Molecular viscosity, Pa.s |
| $\Omega$ | Absolute value of vorticity |
| $\rho$ | Density, $Kg/m^3$ |
| $\omega$ | Specific turbulence dissipation rate, $s^{-1}$ |

*Suffix*

| | |
|---|---|
| $\infty$ | Free stream entity |
| $_0$ | Static entity |
| $t$ | Transition onset |
| $s$ | Streamline |

*Abbreviations*

| | |
|---|---|
| AOA | Angle of attack |
| CFD | Computational fluid dynamics |
| LSB | Laminar separation bubble |
| 2D | Two dimensional |
| 3D | Three dimensional |
| SIMPLE | Semi-implicit method for pressure-linked equations |
| SSWT | Small scale wind turbines |
| RANS | Reynolds averaged Navier–Stokes |
| Re | Reynolds number |
| TKE | Turbulent kinetic energy |

conducted by Jones et al. [14] on E423 airfoil, the tape trips improved lift at low angles of attack (AOA) and higher Re range. But drag reduction was observed at lower Re number condition only. Unlike the previous studies, Lance W. Traub [15] reported reduction in lift for most of the cases he studied and improvement in drag was also observed. It implies that the performance of BLT is airfoil dependent and its applicability depends on the relative advantage between lift and drag coefficients and hence effect on $C_l/C_d$ ratios should be studied. For better performance of the BLT, geometry and position of trip should be such that the flow transition to turbulent should be completed within the separation bubble and not after the reattachment [16]. BLT can be sigle 2D trip to multiple complex 3D trip. Multiple as well as 3-D trips produced no clear benefit over single 2-D plain trips [17]. On airfoils with larger separation bubbles, relatively thin trips are more effective in reducing drag. So plain 2D trips are more popular because of simple structure and easy fabrication. Hence detailed study on plain 2D trip is carried out in this paper.

Wind tunnel experiments are quite expensive and require sophisticated instruments to accurately capture flow pattern and visualize LSB. With well developed modern CFD methods and computational power, turbulent and transitional flow can be modelled effectively and accurately [18–23]. Application of numerical simulation can provide deep insight into the flow physics behind LSB and other aerodynamic effect on the performance of airfoil. Due to limited computational requirement, Reynolds Averaged Navier–Stokes (RANS) methods are more efficient and feasible CFD simulation tool for analysing complex flow phenomena. However widely used RANS models such as $k-\omega, k-\varepsilon$, etc assume a fully turbulent regime in entire flow field. Such models are unable to predict the boundary transition and modelling of LSB becomes challenging [19]. At the same time, models such as large eddy simulation (LES) and direct numerical simulations (DNS) are found be predict LSB accurately but these methods are computationally demanding and requires a long calculation time [24–26,23]. Dhawan and Narasimha [27] first introduced the concept of intermittency ($\gamma$) to predict transition and Menter et al. [28] proposed a transition model based on $\gamma$ which could easily be coupled with general CFD codes and consequently been widely used. This model is reported to have a distinct advantage of associating transition modelling with experimental data [29–32] and the same turbulence model is used in the present study.

Application of BLT are less documented for SSWT. At low Re, airfoil's thick boundary layers and viscous effects are complicated by the presence of laminar transitional bubbles [15]. Only limited simulation works have been reported on the effect of BLT over low Re airfoils. Location of LSB formation and its aerodynamic behaviour varies from airfoil to airfoil and no general predictions are available so far. To use an airfoils for certain application, detailed aerodynamic studies are required to assess its performance. Preliminary aerodynamic analysis of airfoils for low Re (100,000) carried out using Xfoil [33,34] indicated that E216 gives high lift to drag ratio at low Re. This makes E216 a good candidate for SSWT. Experimental or numerical results for E216 are limited in literature. Further, LSB formation and its elimination by BLT is airfoil specific. Hence the present work aims to do a detailed aerodynamic analysis and flow structure study including LSB formation for E216 airfoil. The study also includes the possibility of elimination of LSB, if any, using BLT. To understand the physics behind the aerodynamic behaviour with use of BLT, the flow structure around the BLT and flow pattern downstream of the BLT is analysed.

In this article, 2D numerical simulation using ANSYS FLUENT 15.0 is carried out to model LSB formation over the airfoil E216 and the flow behaviour for different AOA are analysed at Re of 100,000 using Menter's $\gamma - Re_\theta$ transition model. Simulation results are validated with wind tunnel experiments. Effect of BLT placement and heights are evaluated for different AOA, with performance characterization accomplished through the simulation. Effect of trip on the boundary layer formation over airfoil and flow around the trip are elucidated for different locations and AOA.

## 2. Methodology

Airfoil E216 (Fig. 1) is a cambered low Re airfoil suitable for SSWT with maximum thickness of 10.4% at $x/c = 26.2\%$ and camber of 4.7% at $x/c = 59\%$. Power generation from wind turbine blade is proportional to $C_l/C_d$ ratio [35]. The airfoil is selected


**Fig. 1.** E216 airfoil profile.

based on the highest $C_l/C_d$ ratio among the considered airfoils for xfoil analysis [33] at Re of 100,000.

### 2.1. Experimental and measurement techniques

Experiments are conducted in the subsonic open wind tunnel facility in Aeronautical department of Srinivas Institute of Technology, Manglore (Fig. 2). The tunnel has 600 mm times 600 mm times 2000 mm square cross section with jet uniformity within 1% in the core. The wall boundary layer is approximately 5 mm thick. In the empty test section, the turbulence level is measured to be less than 0.12% over the tunnel operating range.

Airfoil model is made up of fibre reinforced plastic (FRP) with 150 mm in chord length and 600 mm in span. Model is mounted horizontally in the test section. The model is provided with 28 pressure taps of 0.5 mm internal diameter located near the mid-span. 19 pressure taps are located on suction side and 9 taps are located on pressure side as given in Table 1. The taps are connected internally to 0.5 mm SS tubing that exits the model through the centre of 10 mm diameter steel tube provided along the span. Pressure measurements are made using HTC make PM-6202 model electronic differential manometer with measurement range of $\pm 2psi$ and accuracy of $\pm 0.3\%$. The maximum blockage in the tunnel during experiment due to airfoil model is 7%. The blockage corrections are not made on the experimental results, because the blockage effects on the experimental results are negligible when the blockage ratio is less than 10% [36,37].

### 2.2. Experimental uncertainties

Uncertainty of electronic manometer used in the experiment for measuring pressure is ±0.3%. Uncertainty in derived quantity is calculated as explained in reference [38] and are given in Table 2.

### 2.3. Computational method

ICEM-CFD is used in the study to create geometry and mesh. Computational domain used for the simulation is shown in Fig. 3. Total length of the computational domain is set to 25 times the chord length to achieve fully developed flow, whereas the width is kept to 20 times [39]. The resolution of the mesh is higher in the region close to the airfoil where greater computational accuracy is needed, shown in Figs. 4 & 5. As per the requirements of the turbulent models used, the height of the first cell adjacent to the surface is set such that it results in $y^+$ value less than one.

Boundary conditions used during the simulations are as follows: on the airfoil – no slip condition, velocity inlet,wall boundary condition at top and bottom boundaries and pressure outlet. Free stream temperature is set to 308 K, same as the environmental temperature in which baseline experiments were carried out. Other properties of the fluid are calculated accordingly. For Re of 100,000, and airfoil chord length of 0.15 m, free stream inlet velocity of air is calculated to be 10.08 m/s. Flow is considered as incompressible. To solve momentum equations semi-implicit method for pressure linked equations (SIMPLE) algorithm [31] and second

**Fig. 2.** Wind tunnel experimental facility.

**Table 1**
Distance of pressure ports (in mm) from leading edge of the airfoil

| | | | | | | | | | | | | | | | | | | | |
|---|---|---|---|---|---|---|---|---|---|---|---|---|---|---|---|---|---|---|---|
| Upper surface | | | | | | | | | | | | | | | | | | | |
| Port No. | 1 | 2 | 3 | 4 | 5 | 6 | 7 | 8 | 9 | 10 | 11 | 12 | 13 | 14 | 15 | 16 | 17 | 18 | 19 |
| Location (mm) | 0 | 1.5 | 3 | 4.5 | 6 | 9 | 12 | 15 | 18 | 23 | 32 | 41 | 50 | 59 | 68 | 78 | 97 | 117 | 142 |
| Lower surface | | | | | | | | | | | | | | | | | | | |
| Port No. | 20 | 21 | 22 | 23 | 24 | 25 | 26 | 27 | 28 | | | | | | | | | | |
| Location (mm) | 6 | 12 | 23 | 41 | 59 | 78 | 97 | 117 | 135 | | | | | | | | | | |

**Table 2**
Uncertainty in the experiment for derived quantities.

| Quantity | Uncertainty (%) |
|---|---|
| $C_p$ | ±0.43% |
| Velocity | ±0.03% |
| Re | ±1.09% |
| $C_l$ | ±1.21% |
| $C_d$ | ±0.21% |

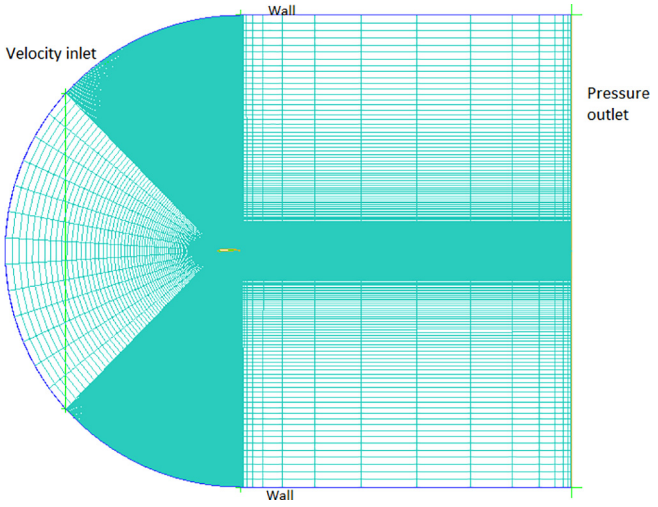


**Fig. 3.** Far view of structured grid in the domain with boundary conditions.

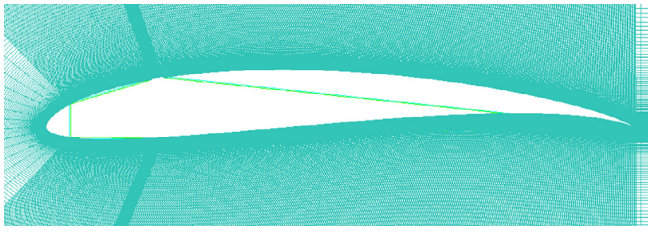

**Fig. 4.** Close view of dense grid around the airfoil.

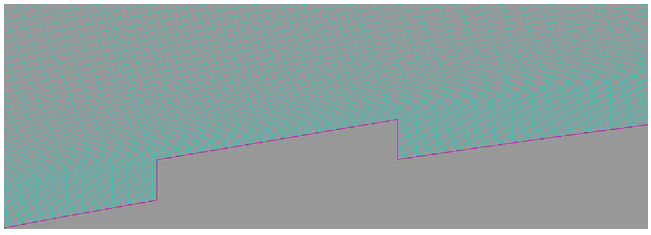

**Fig. 5.** Grid configuration near to BLT.

order upwind spacial discretization is employed in the calculations. Least square cell based spacial gradient is set for spacial gradient. Residual target value of $10^{-6}$ is set as convergence criteria.

### 2.4. Turbulence model

Langtry-Menter 4-equation Transitional SST Model or $\gamma - Re_\theta$ – SST model is used in the study [29]. It is based on the two-equation $k-\omega$ SST model, augmented by two additional equations, one for intermittency ($\gamma$) and another for transitional Reynolds number ($Re_{\theta t}$) to describe the laminar-turbulent transition process. Intermittency term is employed to activate the production term of the turbulent kinetic energy (TKE), downstream of the transition point in the boundary layer, and the Transition Reynolds number term captures the non-local effect of the turbulence intensity [29]. The governing equations involved in this analysis are listed below [29,31,32].

The transport equation for the intermittency term $\gamma$ is given in Eq. (1).

$$\frac{\partial(\rho\gamma)}{\partial t}+\frac{\partial(\rho U_j\gamma)}{\partial x_j}=P_{\gamma 1}-E_{\gamma 1}+P_{\gamma 2}-E_{\gamma 2}+\frac{\partial}{\partial x_j}\left[\left(\mu+\frac{\mu_t}{\sigma_\gamma}\right)\frac{\partial\gamma}{\partial x_j}\right] \quad (1)$$

The transition source terms in the Eq. (1) are,

$$P_{\gamma 1}=2F_{length}\rho S[\gamma F_{onset}]^{c_{\gamma 3}} \quad (2)$$

$$E\gamma 1=P_{\gamma 1}\gamma \quad (3)$$

where $S$ represents the starin rate magnitude and $F_{length}$ is an empirical correlation that controls the length of the transition region. Destruction source terms are given by,

$$P_{\gamma 2}=c_{a2}\rho\Omega\gamma F_{turb} \quad (4)$$

$$E_{\gamma 2}=c_{e2}P_{\gamma 2}\gamma \quad (5)$$

here $\Omega$ represents vorticity magnitude. The functions which control transition onset, $F_{onset}$ are:

$$Re_v=\frac{\rho y^2 S}{\mu} \quad (6)$$

$$R_T=\frac{\rho k}{\mu\omega} \quad (7)$$

$$F_{onset1}=\frac{Re_v}{2.193Re_{\theta c}} \quad (8)$$

$$F_{onset2}=min\left(max\left(F_{onset1},F_{onset1}^4\right),2.0\right) \quad (9)$$

$$F_{onset3}=max\left(1-\left(\frac{R_T}{2.5}\right)^3,0\right) \quad (10)$$

$$F_{onset}=max(F_{onset2}-F_{onset3},0) \quad (11)$$

$$F_{turb}=e^{-\left(\frac{R_T}{4}\right)^4} \quad (12)$$

here $Re_{\theta c}$ is the critical Reynolds number where the intermittency first starts to increase in the boundary layer and $y$ is wall distance. This may find upstream of the transition Reynolds number $\widetilde{Re}_{\theta t}$ and the difference between the two must be obtained from an empirical correlation. Both the $F_{length}$ and $Re_{\theta c}$ correlations are functions of $\widetilde{Re}_{\theta t}$. The terms $Re_v$ is the strain rate Reynolds number, k is the TKE, $\omega$ is specific turbulence dissipation rate and $Re_T$ is viscosity ratio Reynolds number. The value of constants used in the intermittency equations are, $c_{\gamma 1}=0.06; c_{e2}=50; c_{\gamma 3}=0.5$ and $\sigma_\gamma=1.0$.

Equation for transition momentum thickness number, $\widetilde{Re_{\theta t}}$, is given by Eq. (13).

$$\frac{\partial(\rho\widetilde{Re_{\theta t}})}{\partial t}+\frac{\partial(\rho U_j\widetilde{Re_{\theta t}})}{\partial x_j}=P_{\theta t}+\frac{\partial}{\partial x_j}\left[\sigma_{\theta t}(\mu+\mu_t)\frac{\partial\widetilde{Re_{\theta t}}}{\partial x_j}\right] \quad (13)$$

where $P_{\theta t}=c_{\theta t}\frac{\rho}{t}(Re_{\theta t}-\widetilde{Re_{\theta t}})(1.0-F_{\theta t}), t=\frac{500\mu}{\rho U^2}$ and $F_{\theta t}$ is the blending function used to turn off the source term in the boundary layer [31,29,32].

Values of the constants in the Eq. (13) are, $c_{\theta t} = 0.03$ and $\sigma_{\theta t} = 2.0$. In the present work to get better and reliable results, the following values are used in the simulations [40,32];

$c_{\theta t} = 0.02;\ \sigma_{\theta t} = 3.0.$

*2.4.1. Separation – Induced transition correction*

Separation-induced transition can be re written as,

$$\gamma_{sep} = min\left[2.max\left[\left(\frac{Re_v}{3.235Re_{\theta c}}\right) - 1, 0\right]F_{reattach}, 2\right]F_{\theta t} \tag{14}$$

where

$$F_{reattch} = e^{-\left(\frac{R_T}{20}\right)^4}, \tag{15}$$

$$\gamma_{eff} = max(\gamma, \gamma_{sep}) \tag{16}$$

*2.4.2. Coupling the transition model with SST transport equations*

The transition model interacts with the SST turbulence model with modification in the *k*-equation as below:

$$\frac{\partial(\rho k)}{\partial t} + \frac{\partial(\rho u_i k)}{\partial x_i} = \frac{\partial}{\partial x_i}\left(\Gamma_k \frac{\partial k}{\partial x_j}\right) + G_k^* - Y_k^* + S_k \tag{17}$$

where,

$$Y_k^* = min\left(max\left(\gamma_{eff}, 0.1\right), 1.0\right)Y_k \tag{18}$$

and

$$G_k^* = \gamma_{eff} G_k \tag{19}$$

where $Y_k$ and $G_k$ are the terms representing original destruction and production respectively for the SST model. The production term in the $\omega$-equation is used without any modification.

For grid independence test five meshes are prepared with number of grid cells ranging from 1,0,000 to 6,10,000 and simulations are carried out for AOA of $6^0$ and the results are shown in Fig. 6. After around 4,75,000 grid cells there is no significant variation in lift coefficient and hence it is considered as appropriate mesh size for further simulations.

## 3. Results and discussion

Extensive simulations studies are carries out on baseline airfoil E216 at different AOA Re of 100,000 using ANSYS-FLUENT 15.0 and are compared with experimental results obtained from wind tunnel study to validate the computation approach. Experimental or numerical data on E216 is not available in literature and hence validation is done with present experimental data only. Fig. 7 shows the variation of $C_l$ and $C_d$ with AOA obtained from simulations along with experimental results. The simulation results are in good agreement with the experimental measurements especially in the pre-stall region. Numerical results do not exhibit completely satisfactory results in the stall region due to RANS modelling weakness for stalled condition where the flow is highly unsteady [41]. Average deviation of 8.67% in lift prediction and 5.4% in drag prediction is observed between simulation results and experimental results and fall in the acceptable range. The interaction of turbulence models with different combinations of various numerical schemes and grid density may lead to error. The simulations carried out in this study are two dimensional and it cannot capture 3D vortex and its interaction with flow field as it does in experimental study. This also lead to error in results. Reliable matching with least error is obtained in the pre-stall region where the study is mainly focused.

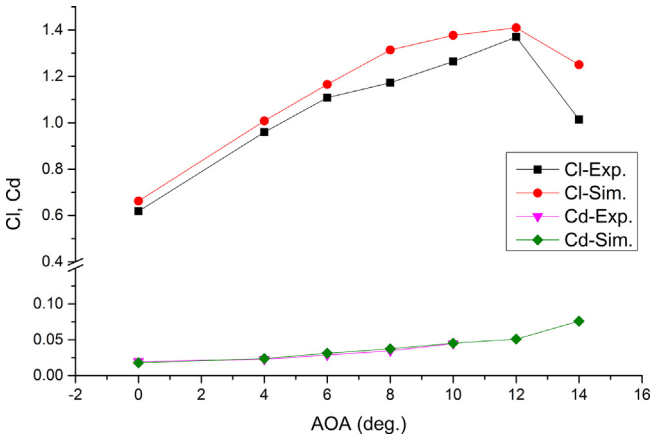


**Fig. 7.** $C_l$ and $C_d$ results obtained from experiment and simulation as a function of AOA.

The simulation result shows that (Fig. 7) $C_l$ curve follows a linear pattern up to maximum value of 1.41 at AOA of $12^0$ and then declines. Upto this maximum $C_l$ value, flow remains attached and the drop in value there after represents separated flow or stalling. Wake survey method is adopted in experiment to measure $C_d$. The method does not give accurate results beyond stalling and hence the experimental $C_d$ measurement is limited up to stall angle.

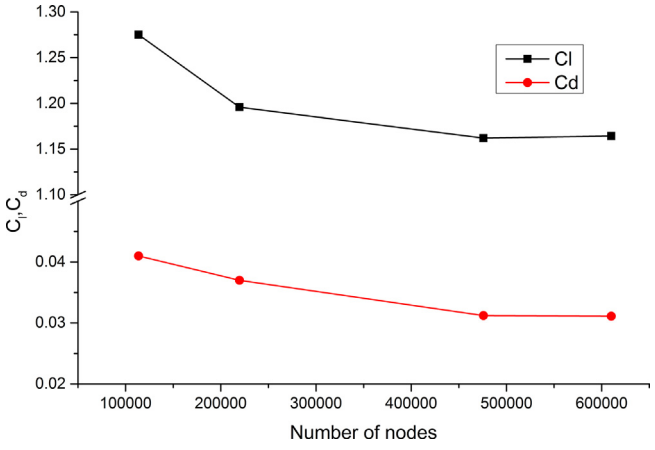


**Fig. 6.** Variation of $C_l$ and $C_d$ of the airfoil for different grid number at AOA of $6^0$.

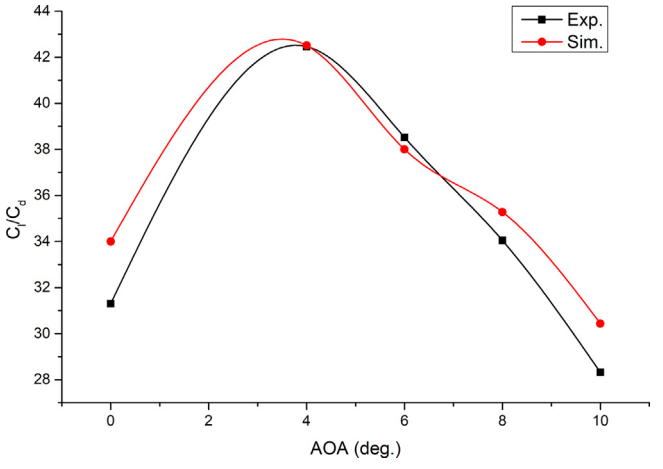


**Fig. 8.** $C_l/C_d$ ratio obtained from experiment and simulation as a function of AOA.

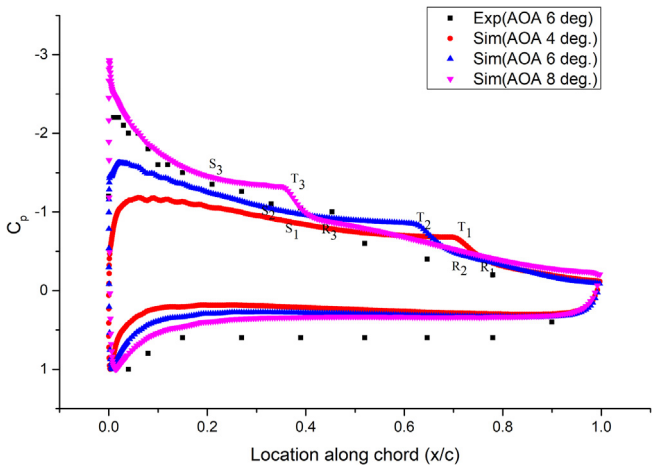


**Fig. 9.** Surface pressure ($C_p$) distribution on the airfoil surface for AOA of: $4^0$ (1), $6^0$ (2) and $8^0$ (3) along with experimental results for AOA of $6^0$. (S – separation point, T – transition point, R – reattachment point).

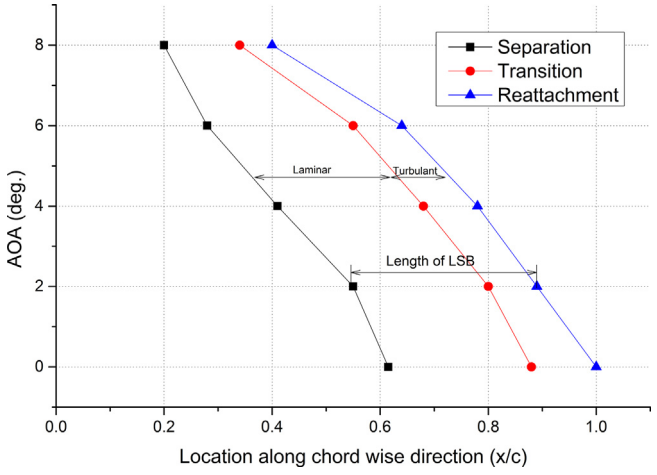


**Fig. 10.** Effect of AOA on size of LSB and its movement along the chord length of the airfoil.

Variation of $C_l/C_d$ ratio with AOA compared with experimental results are shown in Fig. 8. Peak value of 42.50 is observed at AOA of $4^0$ in simulation and value of 42.47 is observed at the same AOA in experiment. Average deviation of 6.57% is observed between experimental and simulation results.

Fig. 9 shows surface pressure distribution over the airfoil for AOA of $4^0, 6^0$ and $8^0$ along with experimental results at AOA of $6^0$. LSB formation can be identified from the presence of pressure plateau in $C_p$ distribution [42]. Both experimental and simulation results clearly depict the presence of LSB, represented by S-T-R points. Points S represent starting of separation (suffixes 1,2 and 3 represent corresponding points for different AOA of $4^0, 6^0 and 8^0$ respectively). Separated flow get mixed up with adjacent laminar layers and forms transition region – represented by T-R curve and the flow is converted to turbulent. When the flow re-energise enough, it attaches back to airfoil surface at point R followed by attached flow represented by smooth $C_p$ distribution there after. For $6^0$ AOA, LSB started from x/c = 0.27 and reattached at x/c = 0.64 and is in good agreement with experimental results.

In order to further investigate the behaviour of LSB, location of separation, transition and reattachment point along airfoil chord length for different AOA are plotted which is shown in Fig. 10. Along with the movement of LSB towards leading edge with increase in AOA, contraction of size is also observed. Increase in AOA results in shortening of laminar region and turbulent region of the LSB. Reduction in turbulent region results in very steep pressure rise. The longest LSB is observed for AOA of $0^0$ which covers 38.5% of chord length and shortest LSB of length 20% of chord length is observed at $8^0$.

Extent of separation and reattachments can also be observed in the velocity vector plot for AOA $6^0$ in Fig. 11. Here the LSB formation can be identified by reversed velocity vector. Close view of the same is shown in Fig. 12 where the reversal of velocity vectors and recirculation are clearly visible.

Based on the simulation results for baseline (Figs. 9 & 11), trip is fixed at two different locations 0.17c (location-1) and 0.10c (location-2) with different trip heights of 0.3 mm, 0.5 mm, 0.7 mm and 1 mm. Simulation is carried out for three different AOA, $4^0, 6^0$ and $8^0$ at Reynolds number of 100,000.

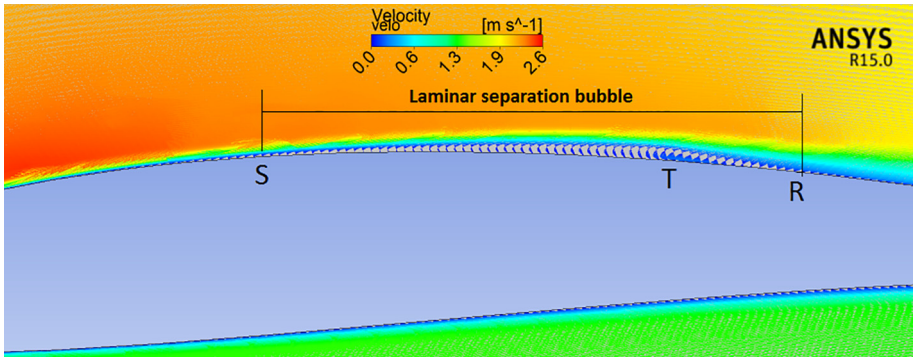


**Fig. 11.** LSB formation over airfoil for AOA of $6^0$ (velocity vector plot).

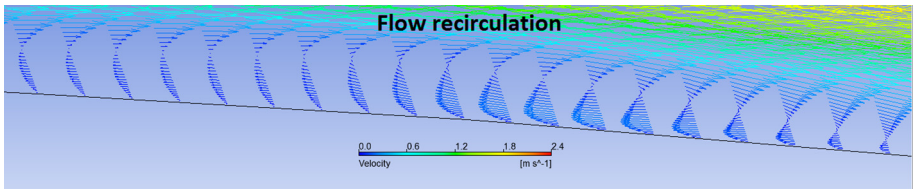


**Fig. 12.** Close view of LSB showing recirculation region at AOA of $6^0$ (where the reversed velocity vector direction shows recirculation flow transition).

### 3.1. Airfoil with boundary layer trips

In this section the effect of BLT on airfoil performance is discussed based on simulation results.

$C_p$ distribution around airfoil for AOA of $4^0$ with trip at location-1 and 2 are shown in Fig. 13a & b respectively. A sudden jump in $C_p$ on suction side near to the trip is due to the flow obstruction caused by the trip. The blockage made the flow to accelerate over

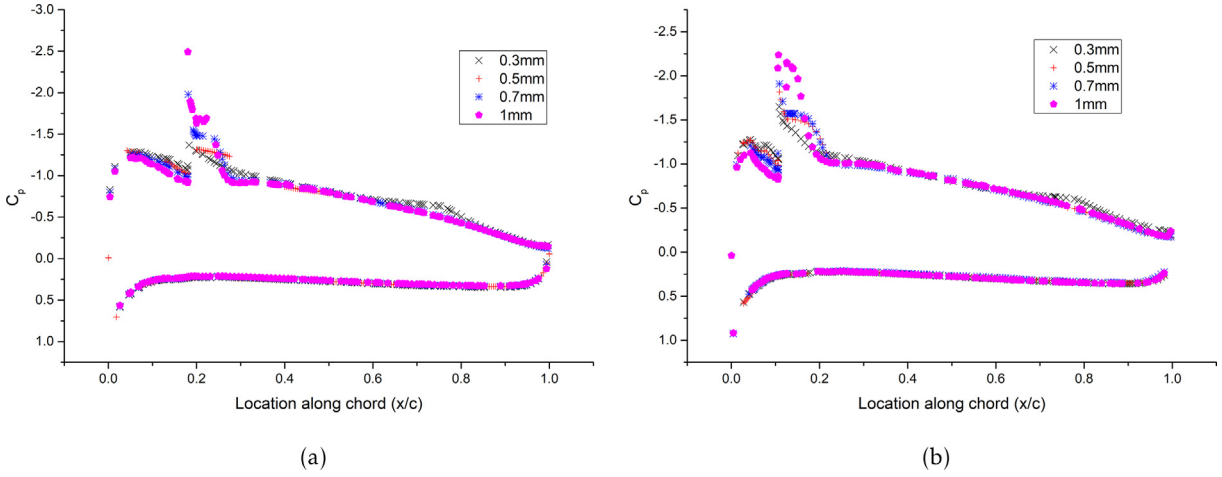


**Fig. 13.** $C_p$ distribution on the airfoil surface for AOA of $4^0$: (a) trip at location-1 and (b) trip at location-2.

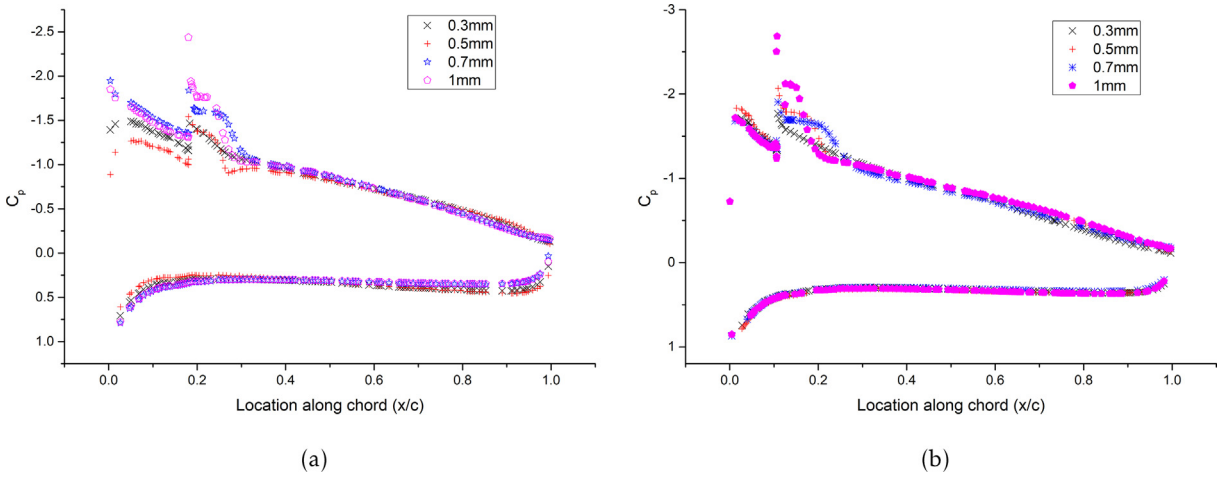


**Fig. 14.** $C_p$ distribution on the airfoil surface for AOA of $6^0$: (a) trip at location-1 and (b) trip at location-2.

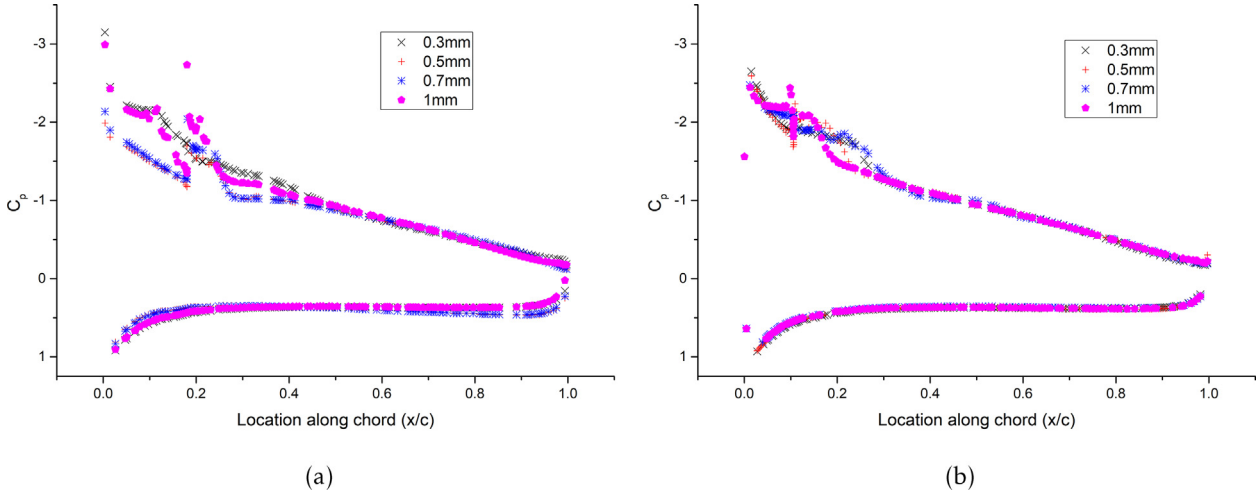


**Fig. 15.** $C_p$ distribution on the airfoil surface for AOA of $8^0$: (a) trip at location-1 and (b) trip at location-2.

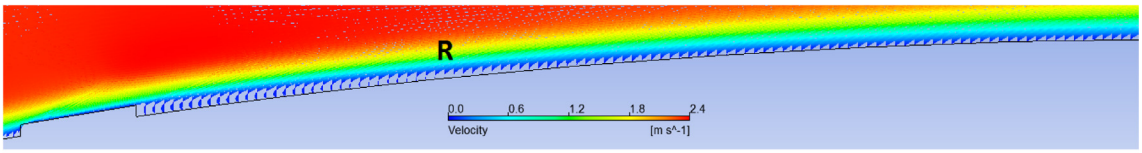


(a) 0.3 mm trip height

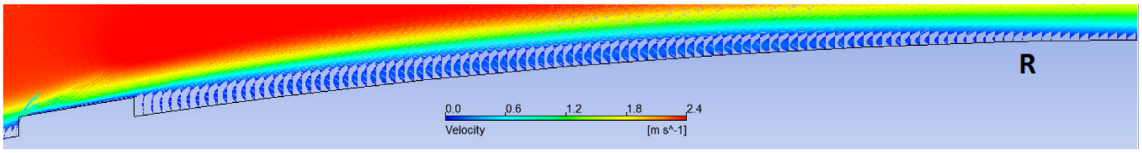


(b) 0.5 mm trip height

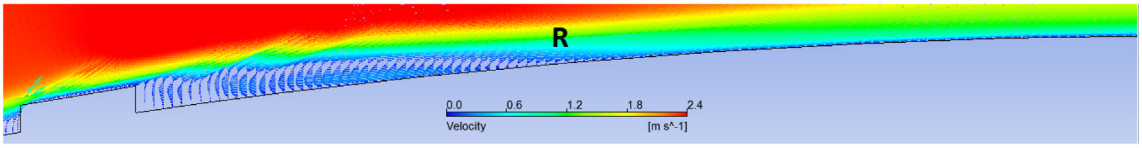


(c) 0.7 mm trip height

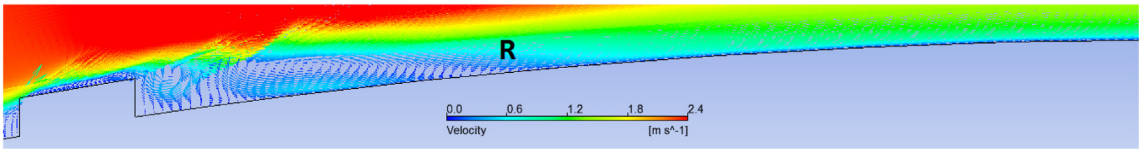


(d) 1 mm trip height

**Fig. 16.** Velocity vector plot over the airfoil at AOA $4^0$ and different trip heights for location-1 (R represents reattachment location).

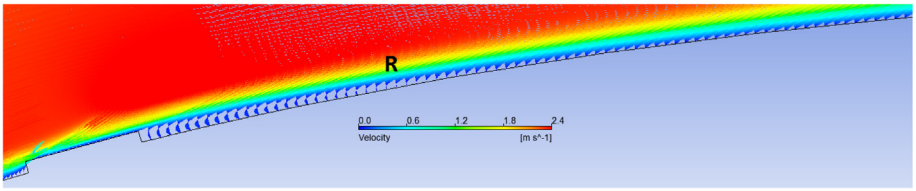


(a) 0.3 mm trip height

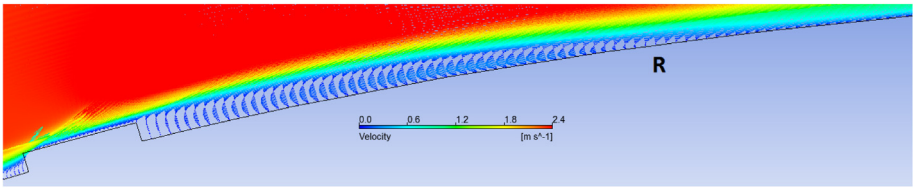


(b) 0.5 mm trip height

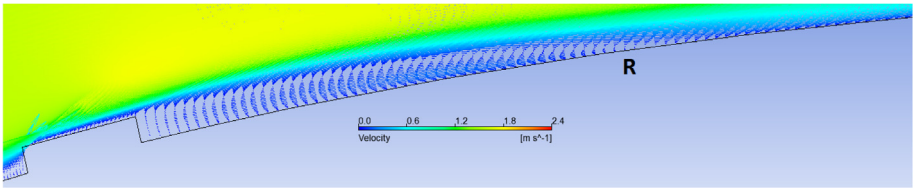


(c) 0.7 mm trip height

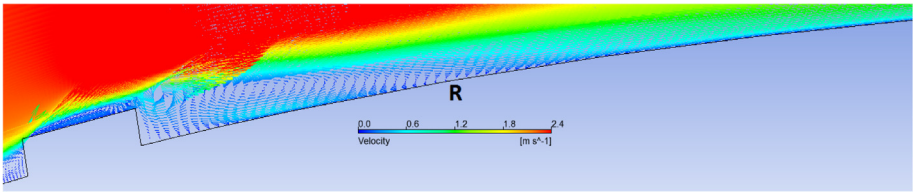


(d) 1 mm trip height

**Fig. 17.** Velocity vector plot over the airfoil at AOA $4^0$ and different trip heights for location-2 (R represents reattachment location).

the trip creating a peak in the $C_p$ distribution. Flow decelerates just after the trip and pressure distribution coincide with normal trend. The distribution becomes smooth there after till the trailing edge, indicating elimination of LSB except for trip height 0.3 mm in both the locations. In case of 0.3 mm trip height at both the locations-1 & 2, the turbulence induced by the trip is insufficient to fully eliminate LSB formation and hence a weak pressure plateau region can be observed in the $C_p$ plot compared to baseline. The $C_p$ distribution over the airfoil surface with BLT at AOA $6^0$ is shown in Figs. 14a & b. Location of LSB on base airfoil is at 0.27c from leading edge as shown in Fig. 9. The figures show that $C_p$ distribution on suction surface with trip is smooth except near the trip, which indicates that the trip successfully transited laminar flow to turbulent with sufficient turbulence. It is clear from the graph that trip eliminated LSB for all the trip heights and trip locations by successfully transiting laminar flow to turbulent. LSB is observed at distance of 0.20c from leading edge in the simulation on base airfoil for AOA of $8^0$. Trip in location-1 is very nearer to LSB. But still it eliminated LSB for all the trip heights (Fig. 15a). $C_p$ distribution over suction surface with trip at location-2 is also smooth as in the previous cases and it does not show any traces of LSB (Fig. 15b).

Figs. 16 & 17 show the velocity vector plots for airfoil with BLT for AOA of $4^0$. Except for 0.3 mm trip height, for all other trip heights the velocity vectors remain attached to the airfoil surface after passing over the trip and there is no sign of LSB formation. A recirculation region is observed just after the trips, where the transition of boundary layer from laminar to turbulent occurs. This transition length reduces as the trip height increased due to the higher induced vortex.

The above discussion shows that trip is effective in reduction/elimination of LSB over the airfoil considered in the study. Net drag reduction is the sum of reduced drag from the elimination of LSB, increased device drag due to the trip blockage and increased skin friction drag due to flow turbulence. Aerodynamic performance analysis is carried out further to quantify the net effect of BLT on the performance the airfoil.

### 3.1.1. Aerodynamic force analysis

Fig. 18a shows the variation of $C_d$ with BLT height at AOA of $4^0$. LSB in baseline airfoil at AOA $4^0$ is observed at a distance of 0.40c from leading edge. Trip is fixed at distances of 0.17c and 0.10c respectively for location −1 & 2 from leading edge. When trip is introduced on airfoil, it converts laminar flow to turbulent. This turbulent flow remains attached to airfoil surface and it avoids/reduces LSB formation. This LSB elimination results in reduced bubble drag. Up to trip height of 0.5 mm, the reduction in bubble

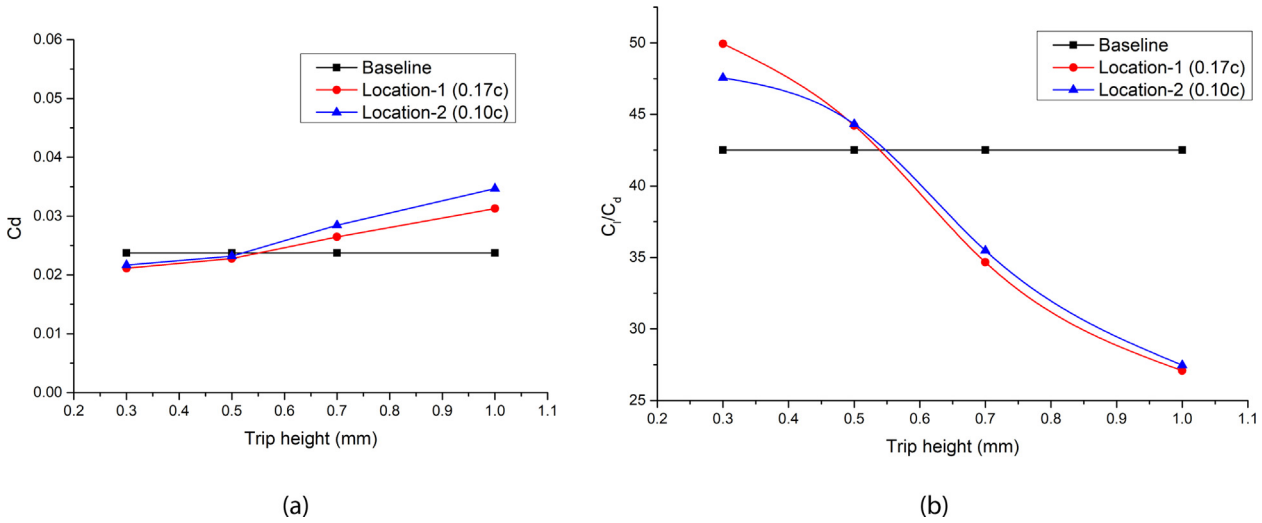


**Fig. 18.** Effect of trip height and location on (a) $C_d$ and (b) $C_l/C_d$ of airfoil at AOA = $4^0$.

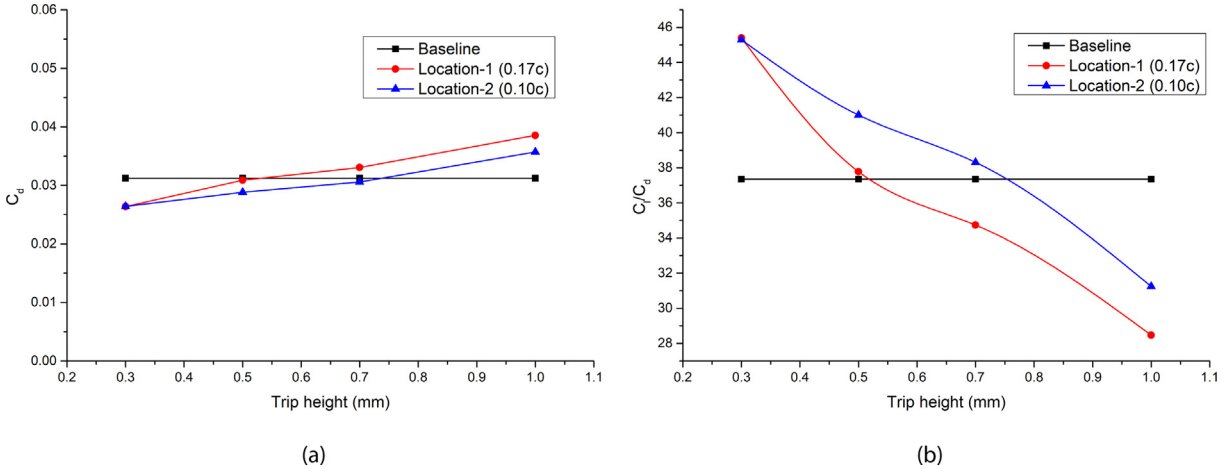


**Fig. 19.** Effect of trip height and location on (a) $C_d$ and (b) $C_l/C_d$ of airfoil at AOA = $6^0$.

drag dominates the increase in frictional drag from the turbulent flow and induced device drag due to trip. Hence, Compared to baseline, tripped airfoil shows better performance up to trip height of 0.5 mm. Thereafter the induced device drag increases with trip height results in nullifying the advantage obtained from reduction in bubble drag. So the total drag becomes higher than baseline airfoil for trip height more than 0.5 mm. Trip at location-2 is located far upstream compared to location-1. So the turbulent flow has to flow longer distance over the airfoil than that for location-1. The laminar flow length before trip is shorter for trip at location-2 and turbulent region is longer compared to location-1. So larger frictional drag is induced for trip at location-2 compared to

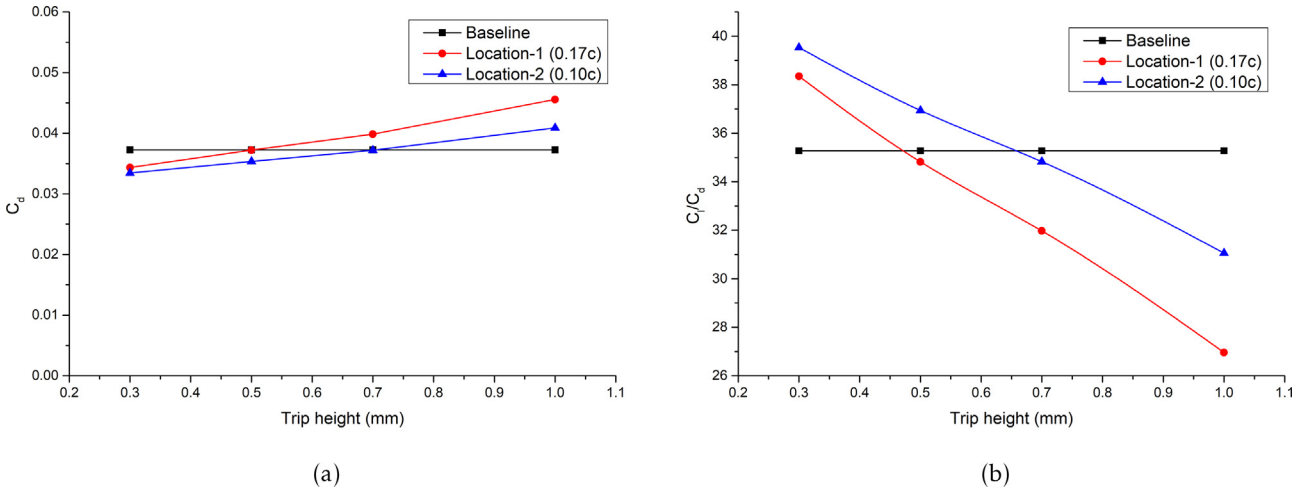


**Fig. 20.** Effect of trip height and location on (a) $C_d$ and (b) $C_l/C_d$ of airfoil at AOA = $8^0$.

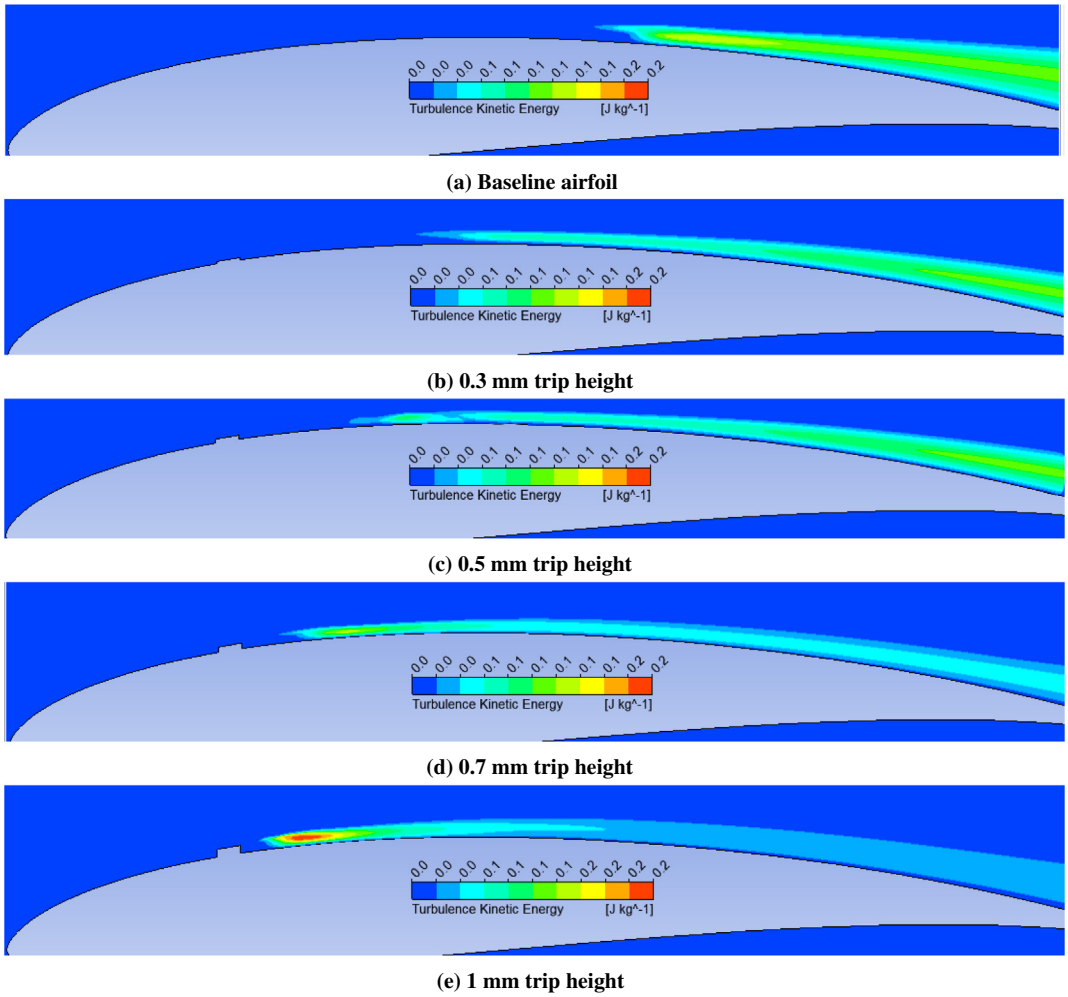


**Fig. 21.** Turbulent kinetic energy (TKE) distribution on base airfoil (21a) and airfoil with boundary layer trip of different heights (21b–e) at location-1 and AOA of $6^0$.

location-1. This results in $C_d$ curve for location-1 to remain always below than that for location-2. The modified model has better $C_l/C_d$ ratio value for both the trip locations up to trip height of 0.5 mm and is shown in Fig. 18b. Trip at location-1 performs better than at location-2 within this limit. For higher trip heights, performance degraded due to the higher induced device drag and it outweighs the advantage obtained from the control of LSB formation.

When the AOA increased to $6^0$ up to trip height of 0.5 mm for location-1 and up to 0.7 mm for location-2, sum of induced device drag and skin friction drag are lesser than reduction in drag achieved by eliminating LSB (bubble drag) using the BLT and net improvement in $C_d$ is observed as shown in Fig. 19a. For higher trip heights induced device drag dominate over reduction in bubble drag. Trip at location-2 is far upstream from LSB than that at location-1. Hence trip at location-2 could induce sufficient turbulence than the trip at location-1 which in turn reduced bubble drag more effectively and hence produce lesser total drag than that in location-1. Maximum improvement in $C_d$ by 15.5% is observed for trip height of 0.3 mm. As the distance between the location of LSB and BLT are more, 'critical height' of trip is also increased. Effect of trip on $C_l/C_d$ ratio is presented in Fig. 19b. As in the case for $C_d$, higher $C_l/C_d$ up to height of 0.5 mm for location-1 and up to 0.7 mm for location-2 are observed than baseline. Maximum improvement of 21.62% is observed at trip height of 0.3 mm. Except for trip height of 0.3 mm, in all other cases location-2 has more advantage over the other.

At AOA of $8^0$ similar trend is observed as that for AOA $6^0$ as shown in Fig. 20a & b. As the AOA increased to $8^0$, LSB moved upstream and the distance between LSB and trip at locations- 1 and 2 got reduced. This results in relatively slight dimnish in drag reduction than that at AOA $6^0$ compared to their corresponding baselines. Maximum reduction in $C_d$ by 10.22% is obtained with 0.3 mm trip height. The same reason holds good for the reduction in $C_l/C_d$ ratio beyond trip height of 0.7 mm compared to baseline.

Fig. 21a shows the distributions of turbulent kinetic energy (TKE) baseline airfoil at AOA of $6^0$. High TKE is observed at a distance of 0.6c from leading edge, where the flow reattaches on the airfoil surface after the LSB formation. It indicates turbulent flow persist after the LSB. The trip induces turbulence into flow and some flow length (transition region) is required for transition into turbulence. Region of high TKE starts where flow reattaches to the airfoil surface after transition. The distance between trip aft and region of high TKE reduces with increase in trip height as shown in Fig. 21b–e. Airfoil with highest trip height have least transition length. Higher the trip height, higher turbulence will be induced and hence shorter transitional length. From the figure it is clear that trip energized the flow by converting laminar flow to turbulent and eliminated high turbulent region due to LSB formation.

## 4. Conclusion

In the work, Simulation studies are carried out to analyse aerodynamic performance of E216 airfoil using Transition $\gamma - Re_\theta$ model. Formation of LSB is modelled and its behaviour under different AOA are studied. Simulation of the airfoil with BLT at different locations and heights, and its effect on LSB formation are also analysed. Clear region of separation, transition and reattachment are observed in the simulation. LSB moved upstream with increase in AOA. When BLTs were introduced on the airfoil, because of induced turbulence, LSB get eliminated in majority of the cases. As height of trip increased, flow reattachment length got reduced after the flow deflection caused by trip obstacle to the flow. If the location of trip is far upstream of LSB, the advantage reduces compared to that when the trip is near to LSB. Though higher trip height eliminated LSB more effectively, the induced device drag is very high which results in performance degradation and trip up to height 0.5 mm is found to perform well. maximum improvement of 21.62% in $C_l/C_d$ ratio is obtained up to trip height of 0.5 mm compared to baseline. There exists an optimum trip height and location for each angle of attack, to achieve maximum improvement in aerodynamic performance of airfoil. But the method is not effective for the applications having wide range of AOA during operation. The presence of trip induce a pressure jump around the trip. The pressure jump can be reduced by selecting an appropriate trip geometry. 3D studies are required to completely understand the vortex structure formation and flow interaction in span-wise direction.

## Acknowledgements

The authors gratefully acknowledge the Aeronautical department of Srinivas Institute of Technology, Mangaluru, Karnataka – India for providing wind tunnel facility in their network.

## References

[1] IEC Standard. 61400-2, 2006. design requirements for small wind turbines. International Electrotechnical Commission, 2, 2006.
[2] Sathyajith Mathew, Geeta Susan Philip, Advances in wind energy and conversion technology, Vol. 20, Springer, 2011.
[3] P.D. Clausen, D.H. Wood, Research and development issues for small wind turbines, Renewable Energy 16 (1) (1999) 922–927.
[4] P.B.S. Lissaman, Low-reynolds-number airfoils, Annu. Rev. Fluid Mech. 15 (1) (1983) 223–239.
[5] William A. Sirignano, Small wind turbines: Analysis, design, and application, AIAA J. 51 (8) (2013). 2045–2045.
[6] G.J. Walker, The role of laminar-turbulent transition in gas turbine engines: a discussion, ASME 1992 International Gas Turbine and Aeroengine Congress and Exposition, pages V001T01A108–V001T01A108, American Society of Mechanical Engineers, 1992.
[7] Ronit K. Singh, M. Rafiuddin Ahmed, Blade design and performance testing of a small wind turbine rotor for low wind speed applications, Renewable Energy 50 (2013) 812–819.
[8] W.D. Musial, D.E. Cromack, Influence of reynolds number on performance modeling of horizontal axis wind rotors, J. Solar Energy Eng. 110 (2) (1988) 139–144.
[9] Ulrich Rist, Kai Augustin, Control of laminar separation bubbles using instability waves, AIAA J. 44 (10) (2006) 2217.
[10] M. Serdar Genc, Ilyas Karasu, H. Hakan Acikel, M. Tugrul Akpolat, M. Genc, Low reynolds number flows and transition. Low Reynolds Number Aerodynamics and Transition, Genc, MS Ed.; InTech: Rijeka, Croatia, pages 1–28, 2012.
[11] Ashok Gopalarathnam, Benjamin A. Broughton, Bryan D. McGranahan, Michael S. Selig, Design of low reynolds number airfoils with trips, J. Aircraft 40 (4) (2003) 768–775.
[12] Tim McCrossen, Aaron Zakrzewski, Trevor Pollock. Boundary layer trips on a clark y12 airfoil at low reynolds numbers. 2010.
[13] Tao Bai, Jingyuan Liu, Weihao Zhang, Zhengping Zou, Effect of surface roughness on the aerodynamic performance of turbine blade cascade, Propulsion Power Res. 3 (2) (2014) 82–89.
[14] A.R. Jones, N.M. Bakhtian, H. Babinsky, Low reynolds number aerodynamics of leading-edge flaps, J. Aircraft 45 (1) (2008) 342–345.
[15] W. Lance, Traub. Experimental investigation of the effect of trip strips at low reynolds number, J. Aircraft 48 (5) (2011) 1776–1784.
[16] M.P. Simens, A.G. Gungor, Influence of the transition of a laminar separation bubble on the downstream evolution of strong adverse pressure gradient turbulent boundary layers, Eur. J. Mech.-B/Fluids 67 (2018) 70–78.
[17] Lyon Christopher A, Selig Michael S, Broeren Andy P, Boundary layer trips on airfoils at low reynolds numbers, AIAA Paper 511 (1997) 35.
[18] H. Medina, A. Beechook, H. Fadhila, S. Aleksandrova, S. Benjamin, A novel laminar kinetic energy model for the prediction of pretransitional velocity fluctuations and boundary layer transition, Int. J. Heat Fluid Flow 69 (2018) 150–163.
[19] A. Crivellini, V. D'Alessandro, D. Di Benedetto, S. Montelpare, R. Ricci, Study of laminar separation bubble on low reynolds number operating airfoils: Rans modelling by means of an high-accuracy solver and experimental verification, Journal of Physics: Conference Series, 501, IOP Publishing, 2014, p. 012024.
[20] Chunhua Sheng, Transition Model, pages 21–54. Springer International Publishing, Cham, 2017.
[21] Guillaume Fournier, Amer Chpoun, Yann Fraigneau, Christian Tenaud, Direct numerical simulations of the shock-induced separation of a laminar boundary layer, in: Direct and Large-Eddy Simulation X, Springer, 2018, pp. 327–332.
[22] M. Sheikholeslami, D.D. Ganji, Heat transfer enhancement in an air to water heat exchanger with discontinuous helical turbulators; experimental and numerical studies, Energy 116 (2016) 341–352.

[23] Mohsen Sheikholeslami and Davood Domiri Ganji, Turbulent heat transfer enhancement in an air-to-water heat exchanger, Proceedings of the Institution of Mechanical Engineers, Part E: Journal of Process Mechanical Engineering 231 (6) (2017) 1235–1248.
[24] Boudet Jérôme, Monier J-F, Gao Feng, Implementation of a roughness element to trip transition in large-eddy simulation, J. Therm. Sci. 24 (1) (2015) 30–36.
[25] Francois Cadieux, Julian A. Domaradzki, Taraneh Sayadi, Sanjeeb Bose, Direct numerical simulation and large eddy simulation of laminar separation bubbles at moderate reynolds numbers, J. Fluids Eng. 136 (6) (2014) 060902.
[26] M. Sheikholeslami, D.D. Ganji, Heat transfer improvement in a double pipe heat exchanger by means of perforated turbulators, Energy Convers. Manage. 127 (2016) 112–123.
[27] S.J. Dhawan, R. Narasimha, Some properties of boundary layer flow during the transition from laminar to turbulent motion, J. Fluid Mech. 3 (4) (1958) 418–436.
[28] Florian R. Menter, Robin Blair Langtry, S.R. Likki, Y.B. Suzen, P.G. Huang, S. Völker, A correlation-based transition model using local variables–part i: model formulation, J. Turbomachinery 128 (3) (2006) 413–422.
[29] F.R. Menter, R. Langtry, S. Völker, Transition modelling for general purpose cfd codes, Flow Turbulence Combust. 77 (1–4) (2006) 277–303.
[30] Robin B. Langtry, Florian R. Menter, Correlation-based transition modeling for unstructured parallelized computational fluid dynamics codes, AIAA J. 47 (12) (2009) 2894–2906.
[31] FLUENT. 15.0. Theory Guide, 2014.
[32] Haseeb Shah, Sathyajith Mathew, Chee Ming Lim, Numerical simulation of flow over an airfoil for small wind turbines using the $\gamma$-$Re_\theta$ model, Int. J. Energy Environ. Eng. 6 (4) (2015) 419–429.
[33] Mark Drela, Harold Youngren, Xfoil 6.94 user guide, 2001.
[34] Mark Drela, Xfoil: An analysis and design system for low reynolds number airfoils, In: Low Reynolds number aerodynamics, pages 1–12. Springer, 1989.
[35] James F. Manwell, Jon G. McGowan, Anthony L. Rogers, Wind Energy Explained: Theory, Design and Application, John Wiley & Sons, 2010.
[36] Scott J. Schreck, Niels N. Srensen, Michael C. Robinson, Aerodynamic structures and processes in rotationally augmented flow fields, Wind Energy 10 (2) (2007) 159–178.
[37] T.Y. Chen, L.R. Liou, Blockage corrections in wind tunnel tests of small horizontal-axis wind turbines, Exp. Thermal Fluid Sci. 35 (3) (2011) 565–569.
[38] Stephen J. Kline, F.A. McClintock, Describing uncertainties in single-sample experiments, Mech. Eng. 75 (1) (1953) 3–8.
[39] Douvi C. Eleni, Tsavalos I. Athanasios, Margaris P. Dionissios, Evaluation of the turbulence models for the simulation of the flow over a national advisory committee for aeronautics (naca) 0012 airfoil, J. Mech. Eng. Res. 4 (3) (2012) 100–111.
[40] K.A. Fagbenro, M.A. Mohamed, D.H. Wood, Computational modeling of the aerodynamics of windmill blades at high solidity, Energy Sustainable Dev. 22 (2014) 13–20.
[41] H. Rahimi, W. Medjroubi, B. Stoevesandt, J. Peinke, 2d numerical investigation of the laminar and turbulent flow over different airfoils using openfoam, Journal of Physics: Conference Series, 555, IOP Publishing, 2014, p. 012070.
[42] J. Russell, Length and bursting of separation bubbles: a physical interpretation. In Science and Technology of Low Speed Motorless Flight, NASA Conference Publication, Vol. 2085, 1979.